Ultrafast laser ablation size and recast adjustment in dielectrics based on electron dynamics control by pulse train shaping

Chuancai Xu (徐传彩)[1], Lan Jiang (姜 澜)[1*], Ni Leng (冷 妮)[1], Yanping Yuan (袁艳萍)[1], Pengjun Liu (刘鹏军)[1], Cong Wang (王 聪)[1], and Yongfeng Lu (陆永枫)[2]

[1]*Laser Micro/Nano-Fabrication Laboratory, School of Mechanical Engineering, Beijing Institute of Technology, Beijing 100081, China*

[2]*Department of Electrical Engineering, University of Nebraska-Lincoln, Lincoln, NE 68588-0511, USA*

[*]*Corresponding author: jianglan@bit.edu.cn*

Received December 12, 2012; accepted December 25, 2012; posted online March 20, 2013

The manipulation of the subpulse number, pulse delay, and pulse energy distribution of an ultrafast laser enables electron dynamics control by changing absorptions, excitations, ionizations, and recombinations of electrons, which can result in smaller, cleaner, and more controllable structures. This letter experimentally reveals that ablation sizes and recasts can be controlled by shaping femtosecond pulse trains to adjust transient localized electron dynamics, material properties, and corresponding phase change mechanisms.

OCIS codes: 140.3390, 320.7130, 320.5540.
doi: 10.3788/COL201311.041403.

Ultrafast lasers are unique tools for processing dielectrics that have drawn increasing attention due to their applications in surface and internal macro/nano processing[1−5]. The ultrashort pulse duration of a femtosecond laser is shorter than or equal to many physical/chemical characteristic times, which offers the capabilities to manipulate, adjust, and/or interfere transient localized electron dynamics, such as excitations, ionizations, recombinations, densities, and temperatures of electrons, using femtosecond laser pulse trains[6−10]. Recent developments in optical devices provide the possibility of obtaining almost any arbitrary pulse shape[11−14]. In using shaped pulse trains, the ionization process can be controlled[15]; atoms can be selectively ionized[16]; the molecular ground-state rotational dynamics can be manipulated[17]; chemical reactions can be controlled[18]; the X-ray line emission from plasmas under a femtosecond pulse can be significantly enhanced[19].

A large number of studies on pulse shaping and its effects on laser-dielectric interactions[20−24] have been reported. Stoian *et al.*[20,21] proposed experiments using temporally shaped femtosecond laser pulses, in which the relationship of the damage threshold with pulse delay was studied, with demonstrated high-quality micromachining. Pump-probe experiments on double-pulse irradiation of dielectrics[22,23] indicate an important dependence of the damage threshold on pulse delay. Furthermore, the influence of temporally asymmetric pulse shapes on the material damage threshold has been investigated[24]. The feasibility of controlling electron dynamics by shaping femtosecond pulse trains has been theoretically validated[25,26]. In addition, preliminary experiments have been performed to validate the theoretical results and the proposed idea[27,28]. However, comprehensively understanding the fundamentals in complex nonequilibrium and nonlinear ablation processes in terms of electron dynamics remains a big challenge. Broad applications based on the electron dynamics control of ultrafast pulse trains require extensive investigation.

In the present experiments, the evolution of the ablation sizes and recasts for the processing of dielectrics (fused silica) using femtosecond pulse trains is investigated. The parameters, such as the subpulse number, pulse delay, and pulse energy distribution, are adjusted. During the processes, the photon-electron interactions and transient localized electron dynamics are adjusted by shaping the femtosecond pulse train, including photon absorption, electron excitation, electron recombination, electron density, electron temperature, and free electron distribution; consequently, the structure size and surface morphology changed. The developed plasma model[29,30] is employed to describe the electron dynamics. The model demonstrates that by shaping femtosecond pulse trains: localized transient electron density can be adjusted and corresponding material properties and phase change mechanisms can be changed; thus, ablation sizes and recasts can be controlled.

The experimental setup included a 35-fs, 800-nm Ti: sapphire laser system with a repetition rate of up to 1 kHz and a pulse shaper (BSI MIIPS BOX 640) system. The time delay and pulse shapes were shaped in the temporal domain by a pulse shaper. The methods employed in the pulse shaper and cross-correlation were used to monitor the pulse trains. A half-wave plate combined with a polarizer was used for continuous energy adjustment. The shaped pulses were focused by a 20× objective lens (numerical aperture = 0.45, Olympus) onto the front surface of the fused silica (0.5-mm thickness), which was driven by a computer-controlled manipulation stage with six degrees of freedom. The size of the focus spot is about 2 μm. The surface of the sample was positioned normal to the direction of the incident laser beam in the air at atmospheric pressure and temperature. Surface damage, namely, visible permanent surface modifications, was inspected by a charge-coupled device (CCD) camera. A scanning electron microscope (SEM) and an atomic force

microscope (AFM) were used to characterize the ablation size and surface morphology.

Figure 1 shows a decrease in ablation diameter and depth as the subpulse number per train increases at the same total fluence. Compared with a conventional single femtosecond pulse, the controllable ablation diameter and the controllable minimal ablation depth decrease by 54% and 84%, respectively. The average for each point is determined using six measured data with a standard deviation from 5% to 10%. For clarity, the error bars corresponding to the standard deviation are not shown.

When the dielectric material is irradiated by femtosecond pulses, the free electrons are generated mainly through multiphoton ionization and impact ionization[29−31]. In theory, the plasma model is employed to investigate the pulse train ablation of fused silica, in which quantum theories are used to calculate the time- and space-dependent optical and thermal properties. These properties include electron heat capacity, electron relaxation time, electron conductivity, reflectivity, and absorption coefficient. Details of the plasma model and the free electron generation can be obtained from Refs. [29,30]. The following expression[29,30] derived from the Fokker-Planck equation is used to calculate the free electron density, which introduces the electron decay term to explain the experimental results of the fused silica:

$$\frac{\partial n_{\rm e}(t,r,z)}{\partial t} = \alpha_{\rm i} I(t,r,z) n_{\rm e}(t,r,z) + \delta_N [I(t,r,z)]^N - \frac{n_{\rm e}(t,r,z)}{\tau}, \quad (1)$$

where t is the time; r is the distance to the Gaussian beam axis; z is the depth from the surface of the bulk material; τ is the decay time constant; $n_{\rm e}(t,\ r,\ z)$ is the free electron density; α_i is the avalanche ionization constant; $I(t,\ r,\ z)$ is the laser intensity inside the bulk material; δ_N is the cross-section of the N-photon absorption. The values for fused silica are as follows: $\alpha_{\rm i} = 4 \pm 0.6$ cm^2/J, $\delta_N = 6 \times 10^{8\pm0.9}$ cm^{-3} ps^{-1}(cm^2/TW)^6[34], and $\tau = 60$ fs[2].

The free electrons generated by multiphoton ionization are proportional to I^6, which strongly affects the impact ionization during the subsequent pulse ablation of fused silica. However, free electron recombination co-exists and plays an increasing role as pulse trains are used, which in turn reduces avalanche ionization during the subsequent pulse irradiation(s); consequently, the free electrons are reduced[29,30]. The free electron density, especially the highest electron density, under a multipulse train is relatively lower than that of a single pulse at equal total fluence, as demonstrated in Table 1. A very good agreement is achieved between the theoretical and experimental ablation dimensions using the plasma model proposed in previous studies[29,30]. Therefore, much smaller structures can be obtained using a pulse train control of the electron density, which implies higher ablation precision.

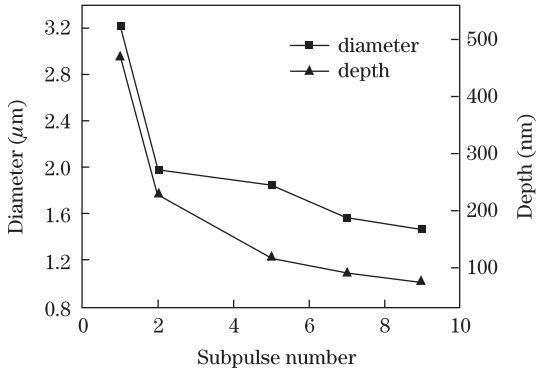

Fig. 1. Pulse number dependence of the ablation diameter and depth for processing fused silica at a pulse delay of 300 fs and 6-J/cm^2 total fluence per train.

Figure 2(a) shows a decrease in recast with the increase in pulse delay. Each point in Fig. 2(a) corresponds to an average value of six data points with a standard deviation from 5% to 10%, which is depicted by error bars. The oscillations in the measured results are due to the experimental uncertainties. Figures 2(b)–(c) show that the recast can be reduced using a temporally shaped femtosecond pulse train. Compared with the results in a conventional single pulse, 60% decrease in the height of recast and 38% decrease in the ratio of the recast height to the pit size are induced by a double-pulse train at 300-fs pulse delay. The recast formation is mainly related to thermal phase changes, especially melting. The model[32] shows the physical processes, which include

Table 1. Pulse-number Dependence of Electron Densities and Ablation Structures

Pulse Number	1	2 (50 fs)	3 (50 fs)
$N_{\rm e}$ ($\times 10^{22}$ cm^{-3})	6.61	4.17	2.20
$D_{\rm T}$ (μm)	2.43	2.08	1.62
$D_{\rm E}$ (μm)	2.87	2.05	1.51

Notes: $N_{\rm e}$: highest total free electron density; $D_{\rm T}$: theoretical ablation diameter calculated by the plasma model; $D_{\rm E}$: experimental ablation diameter.

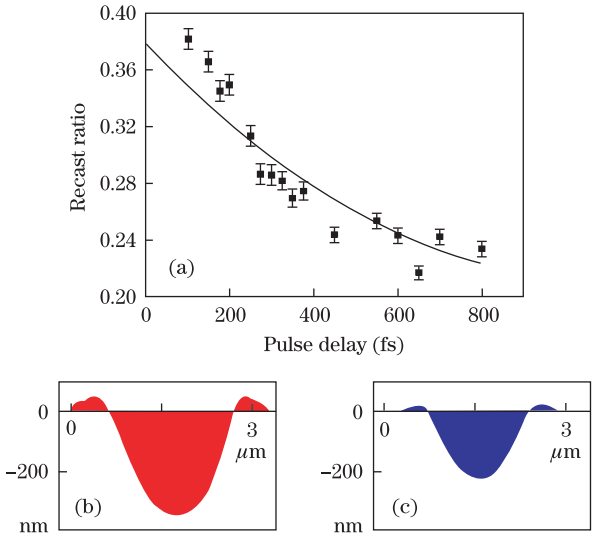

Fig. 2. (a) Pulse delay dependence of the recast ratio (recast area/ablation area) for femtosecond pulse train processing of fused silica by a single burst consisting of two identical subpulses at the same total fluence. AFM profiles of single-burst structures on fused silica: (b) unshaped single pulse, and (c) shaped pulse train excitation with a 300-fs time delay (both with 5-J/cm^2 total fluence).

three main parts: 1) initial nonlinear laser radiation absorption through photon-electron and electron-electron interactions in a time scale from a few femtoseconds to picoseconds; 2) the physics and chemistry of plasma generation and phase change through electron-ion interactions in a time scale from picoseconds to nanoseconds; 3) chemically reactive fluid flow and radiation of expanding plasmas, as well as their interactions with the environment and bulk materials from a few nanoseconds to hundreds of microseconds.

The free electron density decreases as the pulse delay increases[30]. In the case of a single pulse (or if the pulse delay is very short), electron density is much higher than the critical density (n_e) and the Coulomb barrier is high, which leads to significant electron screening effects. This condition reduces the accumulation of positive charge during a femtosecond laser pulse, thus reducing the electric field that decreases the effectiveness of the non-thermal processes (Coulomb explosion and electrostatic ablation). Part of a non-thermal phase change is converted to thermal processes, including melting (different phase change mechanisms coexist in the process), which increases the recasts that are strongly associated with melting. In pulse train processing, when the electron density is slightly higher than n_e, free electrons escape with high kinetic energy and the phase change is mainly dominated by non-thermal processes that reduce the recast. Thus, melting and its associated recast can be minimized by designing femtosecond laser pulse trains to maintain a free electron density that is slightly higher than the critical density.

As shown in the inset of Fig. 3(a), the ablation diameter of fused silica decreases as the pulse delay time increases, which coincides with previous studies[20,21]. As shown in the inset of Fig. 3(b), the diameter changes are due to the adjustments made in the excitations, ionizations, densities, and recombinations of electrons by designing pulse trains, which has been theoretically predicted by previous studies[29,30]. An interesting phenomenon is observed when detailed investigation in the experiments is performed. As shown in Fig. 3, the ablation dimension rises to a peak value at the pulse delay of around 175 fs, followed by a decrease over a time period of 100 fs. At different fluences, the trend is constantly repeatable, as shown in Figs. 3(a)–(b). At a pulse delay of 50 to 300 fs, the ablation diameter is enhanced, which arises from the higher free electron density compared with that of a larger pulse delay. Some electrons excited by the first pulse remain in the conduction band before the next pulse is irradiated because the free electron relaxation time of fused silica is also within the range from 50 to 300 fs. This condition leads to more seed free electrons and contributes to the enhancement of avalanche ionization. Moreover, the previous pulse has significant effects on the thermal and optical properties of the subsequent pulse within the same train[29]. The specific electron density and electron temperature may promote the effective absorption of the pulse energy, which significantly enhances the ablation around the 175-fs pulse delay. Comparisons between conventional single pulse and pulse trains (double pulses and triple pulses per train) with equal total fluence were performed. As shown in Fig. 3(a), smaller structures can

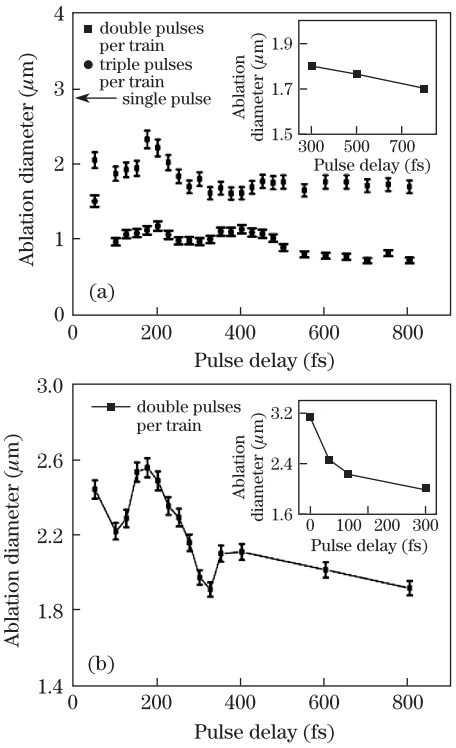

Fig. 3. Pulse delay dependence of the ablation diameters for processing fused silica by a single burst consisting of two identical subpulses: (a) 5-J/cm^2 total fluence per train and (b) 6-J/cm^2 total fluence per train. The insets show the dependence with specific pulse delay.

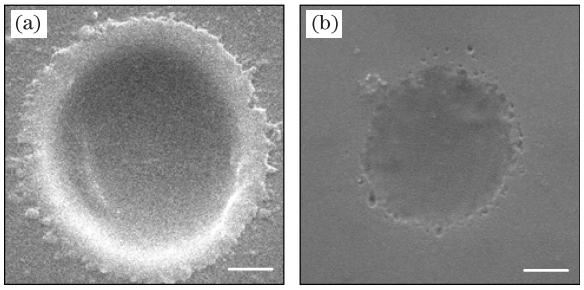

Fig. 4. SEM images of single-burst structures on fused silica by double pulses in a train at a pulse delay of 500 fs and 5-J/cm^2 total fluence. Pulse energy distribution of (a) 1:1 and (b) 2:1. The scale bars indicate 500 nm.

be obtained by the pulse train technology.

The pulse energy distribution is one of the most important parameters of shaped pulse train that has an important function in the processing of dielectrics of femtosecond pulse trains. At the two subpulses with an energy distribution of 2:1 and a delay of 500 fs, the diameter is about 44% smaller compared with that of the 1:1 pulse energy, as presented in Fig. 4. This difference results from the adjustment of the free electron distribution by the pulse train[27], which modulates the multiphoton ionization and avalanche ionization. Furthermore, less absorption of the second subpulse due to the high reflectivity induced by the relatively higher intensity of the first subpulse results in less ablation. However, the relatively weaker intensity of the second subpulse could not provide enough plasma pressure to drive the melt

sufficiently outward to overlap a clearly visible recast (Fig. 4(b)).

In conclusion, the ablation size and recast adjustments are investigated by manipulating the pulse train parameters (including the subpulse number per train, pulse delay, and pulse energy distribution) based on transient localized electron dynamics control. The following results are obtained: 1) structure ablation diameter and depth decrease with the increase in subpulse number per train, such that the controllable ablation diameter and minimal ablation depth decrease by 54% and 84% using the pulse train technology based on electron dynamics control; 2) recasts can be reduced by temporally shaping pulse trains; 3) ablation enhancement exists at a pulse delay from 50 to 300 fs, especially around 175 fs; 4) the ablation diameter decreases by about 44% through shaping the pulse energy distribution. The experimental results demonstrate that the ablation sizes and recasts can be reduced by shaping femtosecond pulse trains to control localized transient electron dynamics, material properties, and corresponding phase change mechanisms. Electron dynamics control provides a promising method for obtaining controllable, small, and repeatable structures depending on the employed pulse train.

This work was supported by the National "973" Program of China (No. 2011CB013000) and the National Natural Science Foundation of China (Nos. 90923039 and 51025521).

References

1. B. C. Stuart, M. D. Feit, A. M. Rubenchik, B. W. Shore, and M. D. Perry, Phys. Rev. Lett. **74,** 2248 (1995).
2. M. Li, S. Menon, J. P. Nibarger, and G. N. Gibson, Phys. Rev. Lett. **82,** 2394 (1999).
3. R. R. Gattass and E. Mazur, Nat. Photon. **2,** 219 (2008).
4. Y. Li, X. Gao, M. Jiang, Q. Sun, and J. Tian, Chin. Opt. Lett. **10,** 102201 (2012).
5. Y. Liao, Y. Ju, L. Zhang, F. He, Q. Zhang, Y. Shen, D. Chen, Y. Cheng, Z. Xu, K. Sugioka, and K. Midorikawa, Opt. Lett. **35,** 3225 (2010).
6. G. Sansone, E. Benedetti, F. Calegari, C. Vozzi, L. Avaldi, R. Flammini, L. Poletto, P. Villoresi, C. Altucci, R. Velotta, S. Stagira, S. De Silvestri, and M. Niso, Science **314,** 443 (2006).
7. A. L. Cavalieri, N. Müller, T. Uphues, V. S. Yakovlev, A. Baltuška, B. Horvath, B. Schmidt, L. Blümel, R. Holzwarth, S. Hendel, M. Drescher, U. Kleineberg, P. M. Echenique, R. Kienberger, F. Krausz, and U. Heinzmann, Nature **449,** 1029 (2007).
8. E. Goulielmakis, V. S. Yakovlev, A. L. Cavalieri, M. Uiberacker, V. Pervak, A. Apolonski, R. Kienberger, U. Kleineberg, and F. Krausz, Science **317,** 769 (2007).
9. E. Goulielmakis, M. Schultze, M. Hofstetter, V. S. Yakovlev, J. Gagnon, M. Uiberacker, A. L. Aquila, E. M. Gullikson, D. T. Attwood, R. Kienberger, F. Krausz, and U. Kleineberg, Science **320,** 1614 (2008).
10. M. Meckel, D. Comtois, D. Zeidler, A. Staudte, D. Pavicic, H. C. Bandulet, H. Pepin, J. C. Kieffer, R. Dorner, D. M. Villeneuve, and P. B. Corkum, Science **320,** 1478 (2008).
11. T. Baumert, T. Brixner, V. Seyfried, M. Strehle, and G. Gerber, Appl. Phys. B **65,** 779 (1997).
12. A. M. Weiner, Rev. Sci. Instrum. **71,** 1929 (2000).
13. S. H. Shim, D. B. Strasfeld, E. C. Fulmer, and M. T. Zanni, Opt. Lett. **31,** 838 (2006).
14. S. Weber, M. Barthelemy, and B. Chatel, Appl. Phys. B **98,** 323 (2010).
15. R. Bartels, S. Backus, E. Zeek, L. Misoguti, G. Vdovin, I. P. Christov, M. M. Murnane, and H. C. Kapteyn, Nature **406,** 164 (2000).
16. A. Lindinger, C. Lupulescu, M. Plewicki, F. Vetter, A. Merli, S. M. Weber, and L. Woste, Phys. Rev. Lett. **93,** 033001 (2004).
17. M. Renard, E. Hertz, B. Lavorel, and O. Faucher, Phys. Rev. A **69,** 043401 (2004).
18. A. Assion, T. Baumert, M. Bergt, T. Brixner, B. Kiefer, V. Seyfried, M. Strehle, and G. Gerber, Science **282,** 919 (1998).
19. A. A. Andreev, J. Limpouch, A. B. Iskakov, and H. Nakano, Phys. Rev. E **65,** 026403 (2002).
20. R. Stoian, M. Boyle, A. Thoss, A. Rosenfeld, G. Korn, I. V. Hertel, and E. E. B. Campbell, Appl. Phys. Lett. **80,** 353 (2002).
21. R. Stoian, M. Boyle, A. Thoss, A. Rosenfeld, G. Korn, and I. V. Hertel, Appl. Phys. A **77,** 265 (2003).
22. Y. P. Deng, X. H. Xie, H. Xiong, Y. X. Leng, C. F. Cheng, H. H. Lu, R. X. Li, and Z. Z. Xu, Opt. Express **13,** 3096 (2005).
23. I. H. Chowdhury, X. F. Xu, and A. M. Weiner, Appl. Phys. Lett. **86,** 151110 (2005).
24. L. Englert, B. Rethfeld, L. Haag, M. Wollenhaupt, C. Sarpe-Tudoran, and T. Baumert, Opt. Express **15,** 17855 (2007).
25. C. Wang, L. Jiang, F. Wang, X. Li, Y. Yuan, and H. L. Tsai, Phys. Lett. A **375,** 3200 (2011).
26. C. Wang, L. Jiang, F. Wang, X. Li, Y. Yuan, H. L. Tsai, and Y. Lu, J. Phys. Condens. Matter **24,** 275801 (2012).
27. L. Jiang, P. Liu, X. Yan, N. Leng, C. Xu, H. Xiao, and Y. Lu, Opt. Lett. **37,** 2781 (2012).
28. N. Leng, L. Jiang, X. Li, C. Xu, P. Liu, and Y. Lu, Appl. Phys. A **109,** 679 (2012).
29. L. Jiang and H. L. Tsai, Appl. Phys. Lett. **87,** 151104 (2005).
30. L. Jiang and H. L. Tsai, J. Heat Tran. **128,** 926 (2006).
31. Y. Yuan, L. Jiang, X. Li, C. Wang, H. Xiao, Y. Lu, and H. L. Tsai, J. Phys. D **45,** 175301 (2012).
32. L. Jiang, L. Li, S. Wang, and H. L. Tsai, Chin. J. Lasers (in Chinese) **36,** 779 (2009).